Chemical Physics 526 (2019) 110414

Contents lists available at ScienceDirect

Chemical Physics

journal homepage: www.elsevier.com/locate/chemphys

Electronic band structure, thermodynamics and optical characteristics of $BeO_{1-x}A_x$(A = S, Se, Te) alloys: Insights from ab initio study

Mohammed M. Obeid[a], Majid M. Shukur[a], Shaker J. Edrees[a], R. Khenata[b,*], M.A. Ghebouli[c], Shakeel Ahmad Khandy[d], A. Bouhemadou[e], Hamad Rahman Jappor[f], Xiaotian Wang[g,*]

[a] Department of Ceramic, College of Materials Engineering, University of Babylon, 51002 Babylon, Iraq
[b] Laboratoire de Physique Quantique de la Matière et de Modélisation Mathématique(LPQ3M), Université de Mascara, 29000, Algeria
[c] Department of Chemistry, Faculty of Technology, University of Mohamed Boudiaf, M'sila 28000, Algeria
[d] Department of Physics, Islamic University of Science and Techonology, Awantipora, Jammu and Kashmir 192122, India
[e] Laboratory for Developing New Materials and their Characterization, University of Setif 1, 19000 Setif, Algeria
[f] Department of Physics, College of Education for Pure Sciences, University of Babylon, Hilla, Iraq
[g] School of Physical Science and Technology, Southwest University, Chongqing 400715, People's Republic of China

ARTICLE INFO

Keywords:
Alloys
Electronic properties
Optical properties
Thermodynamic properties
Ab initio

ABSTRACT

Special quasi-random structure (SQS) was used to investigate the structural, electronic, and optical characteristics of the binary and ternary beryllium chalcogenide alloys. The computations were performed using the pseudopotential technique. The GGA-WC scheme was applied to study the structural and optical features of these present alloys, while the HSE06 hybrid functional was used to correct the underestimation of the electronic band structure. The optimized lattice constants and bulk modulus demonstrate a non-linear tendency with increasing x concentration. The phase transition may occur for all ternary alloys at $x = 0.5$ with the orthorhombic assumed crystal system. The ternary alloys of $BeO_{1-x}A_x$ (A = S, Se) at $0.5 \leqslant x \leqslant 1$ have an indirect band gap, while $BeO_{1-x}Te_x 0.5 \leqslant x \leqslant 1$ manifest a metallic demeanor using HSE06 formalism. The optical spectra were computed and discussed in detail. Furthermore, the thermodynamic stability of the studied compounds was examined using the miscibility critical temperature.

1. Introduction

Alkaline earth oxides, an important substance of metal oxides, crystallize in cubic rocksalt (RS) structure. Beryllium oxide (BeO) is a special type of this series that crystallizes in wurtzite (WZ)structure. It also can be found in zinc blende (ZB) and rocksalt forms at varying pressure [1–3]. Due to its unique crystal, optical, electronic, and thermal features [4–7], BeO can be used in rockets, missiles, atomic energy, aviation, nuclear, and metallurgical applications [8–10]. Beryllium chalcogenides are very attractive compounds for technological applications because of their wide band gap, high bulk modulus, and also they have the same structure and bonding with III-IV semiconductors group [11]. Beryllium chalcogenide BeX (X = S, Se, Te) semiconductors crystallize in the zinc blende (ZB) form at normal conditions [12,13]. The pressure-induced phase transition from ZB (B3) to NiAs (B8) structure for BeTe and BeSe at 35 GPa and 56 GPa, respectively [14]. On the other hand, BeS transforms from (B3) to (B8) at 69 GPa [15].

From an experimental point of view, beryllium oxide transforms directly from wurtzite to rocksalt structure under the influence of pressure [16,17]. Theoretically, Van Camp and Van Doren [18], confirmed that the wurtzite type transforms to zinc blende and rocksalt structure at 74 GPa and 137 GPa, respectively. Based on phonon dispersion, both RS-BeS and RS-BeO are dynamically unstable at zero pressure [19]. The phonon dispersion of rocksalt magnesium oxide MgO can be taken as a reference system for comparison with dynamically stable structures [20]. Furthermore, the phonon dispersion of RS-BeO testified by Guo*et al.* [21] shows no imaginary frequencies at 81.27 GPa, indicating that the RS-BeO structure is dynamically stable at higher pressure. Based on enthalpy versus pressure and common tangent of total energy versus volume curves, Dabhi*et al.* [14]found that the sequence of phase transition from B3 to B1 comes out to be 73 GPa, 59 GPa and 41 GPa for BeS, BeSe, and BeTe, respectively.

Beryllium oxide possesses a wide band gap of about 10.67 eV [22]. Furthermore, Thapa *et al.* [23]investigated the electronic properties of ZB-BeX (X = S, Se, Te) using the FP-LAPW method. They suggested that

* Corresponding authors.
E-mail addresses: khenata_rabah@yahoo.fr (R. Khenata), xiaotianwang@swu.edu.cn (X. Wang).

https://doi.org/10.1016/j.chemphys.2019.110414
Received 9 February 2019; Received in revised form 12 June 2019; Accepted 20 June 2019
Available online 05 July 2019
0301-0104/

BeSe and BeS systems have an indirect band gap, with a metallic behavior for BeTe. Recently, it is possible to estimate the most valuable characteristics of solid materials, such as bandgap structure, elastic constants, optical, and thermodynamic features using quantum mechanical computations [24–30].

In the present work, density functional theory has been used to study in details the structural, electronic, optical, and thermodynamic properties of RS-$BeO_{1-x}A_x$ (A = S, Se, Te) solid solutions. We have used the SQS method, which significantly diminishes the size of the supercell needed in order to find a realistic order of a random alloy. Lately, there has been a consideration in the investigation of these types of alloys, and a few theoretical first-principles calculations have been achieved.

2. Computational method

First-principles analysis was proceeded to employ the plane-wave pseudopotential scheme within the framework of density functional theory (DFT) as implemented in the CASTEP code [31]. The exchange–correlation energy of electrons interaction was treated by means of the Wu-Cohen generalized gradient approximation (GGA-WC) [32]. For geometry optimization, ultra-soft pseudopotentials were used together with a plane-wave cutoff energy of 1000 eV. Brillouin zone (BZ) scheme integration of 14 × 14 × 14 *k*-points by means of Monkhorst-Pack grid [33] was appropriate in making the electron system to converge for pristine binary beryllium chalcogenides. For the ternary alloys, we applied cutoff energy of 800 eV and 32 irreducible *k*-points. Furthermore, finer *k*-point meshes (455 points) were applied to estimate the optical properties of the studied materials. The convergence tolerance adopted for all the geometry optimization in the Broyden-Fletcher-Goldfarb-Shanno (BFGS) algorithm [34] were set asa fine quality with a maximum force of 3×10^{-2} eV/Å. A tolerance of 1×10^{-6} eV/atom with a convergence window of three steps was exploited for the self-consistent calculations. Due to the underestimation of the band gap values using the conventional method based on DFT, HSE06 hybrid function [35,36] was conducted to produce a better exchange and correlation energy. Supercell was built to change the atomic position of the studied alloys. Zunger *et al.* [37] suggested that employing a quasi-random structure technique can reduce the supercell size. This technique can be used to study various properties of alloys [38–40]. Several tests have been done using different values of plane-wave cutoff energy and *k*-points mesh to produce stable final energy. The configuration of valence electrons was $2s^2$ for Be, $2s^22p^4$ for O, $3s^23p^4$ for S, $4s^24p^4$ for Se and $5s^25p^4$ for Te.

3. Results and discussion

3.1. Structural properties

We recorded the optimized lattice parameters and bulk modulus for the parent compounds BeA (A = S, Se, and Te), BeO and ternary $BeO_{1-x}A_x$ (A = S, Se, Te) alloys for x = 0.25, 0.5 and 0.75. At x = 0.25 and 0.75, the optimized structure belongs to the rocksalt structure (space group $Fm\bar{3}m$ no. 225). At x = 0.5, phase transition may occur for all ternary alloys with an orthorhombic assumed crystal system [40]. Their structural characterizations were estimated by using the GGA-WC approximation. Special quasi-random structure (SQS) was employed to create the binary and ternary supercells. The atomic position of ternary alloys at various x concentration are listed in Table 1. We reported in Table 2 the lattice constant of the ternary alloys $BeO_{1-x}A_x$ (A = S, Se, Te) according to the x concentration. The optimized lattice constants of the parent compounds BeA (A = S, Se, and Te) are in acceptable agreement with the previous experimental and theoretical reports [1,14,18,19,41–46]. Our calculated lattice parameters diverge from the standard ones within 2.9, 0.43 and 0.37% for BeO, BeSe, and BeTe, respectively. Consequently, the GGA-WC scheme underestimates the lattice constant. There is no available data for ternary alloys, therefore, our results are predictions. It is obvious that the lattice constant increases when the x fraction increases in $BeO_{1-x}A_x$ (A = S, Se, Te) alloys as presented in Fig. 1. A second polynomial function was used to estimate the lattice constant deviation based on Vegard's rule [47], which revealed that the deviation increases in the sequence S → Se → Te. This can be explained by their large difference in the atomic radius [39,48]. Also, it should be related to the large mismatch of the lattice constants a of the end compounds [49]. This, in turn, may lead to the phase separation even at low x concentration during the synthesis process. However, infraction of Vegard's rule has been stated for semiconductor alloys, both theoretically [50] and experimentally [51,52]. The calculated lattice constants at various concentrations as displayed in Fig. 1, were fitted according to the expression below:

$$a^{BeO_{1-x}A_x} = xa^{BeA} + (1-x)a^{BeO} - bx(1-x)b_d \quad (1)$$

where $a^{BeO_{1-x}A_x}$, a^{BeO} and a^{BeA} are the lattice constants of $BeO_{1-x}A_x$ alloys and their parents BeO, and BeA, correspondingly. The quadratic expression b_d signifies the disordered factor. The achieved values of upward bowing factors (b) are −0.49, −0.708, and −1.33 Å for $BeO_{1-x}S_x$, $BeO_{1-x}Se_x$, and $BeO_{1-x}Te_x$, respectively. Variations of the total energy (E) vs. primitive unit cell volume (V) data were adapted under the Birch-Murnaghan [53] equation of state to evaluate the ground state features of the binary and ternary beryllium chalcogenides, like bulk modulus B_0 and its pressure derivative B'. The values of the bulk modulus B_0 and B' are tabulated in Table 2. The reported values of bulk modulus and its pressure derivative in Table 2 are consistent with the previous theoretical data [1,14,18,42–45]. The variation of the bulk modulus as a function of the alloying concentration x for the $BeO_{1-x}S_x$, $BeO_{1-x}Se_x$, and $BeO_{1-x}Te_x$ compounds are depicted in Fig. 2, and likened to the estimated result by the linear concentration dependence (LCD). A considerable change from the LCD is detected by downward bowing equivalent to 119.4, 160 and 258.4 GPa for $BeO_{1-x}S$, $BeO_{1-x}Se$ and $BeO_{1-x}Te$, respectively. It seems that the deviation from LCD is more significant in the order S → Se → Te, and this may be primarily because of the large bulk modulus mismatch between the end compounds [54]. A comparison of the bulk modulus and lattice parameters of the studied compounds (Figs. 1 and 2) evinces that an augment of the later parameters is followed by a reduction of the former ones. This form of variation depicts the weakening or strengthening result caused by changing the x concentration. There are no experimental data for structural properties to be used as a reference, but our estimated values are comparatively close to those of Park *et al.* [42] and Munoz *et al.* [45].

Table 1
Atomic position of the ternary alloys $BeO_{1-x}A_x$ (A = S, Se, Te).

x	Atom	Position
0.25	**Be**	(0, 0, 0) (0.5, 0.5, 0) (0.5, 0, 0.5) (0, 0.5, 0.5)
	O	(0.5, 0, 0) (0, 0.5, 0) (0, 0, 0.5)
	A	(0.5, 0.5, 0.5)
0.5	**Be**	(0, 0, 0) (0.5, 0.5, 0) (0.5, 0, 0.5) (0, 0.5, 0.5)
	O	(0, 0.5, 0) (0, 0, 0.5)
	A	(0.5, 0, 0) (0.5, 0.5, 0.5)
0.75	**Be**	(0, 0, 0) (0.5, 0.5, 0) (0.5, 0, 0.5) (0, 0.5, 0.5)
	O	(0.5, 0,5, 0.5)
	A	(0.5, 0, 0) (0, 0.5, 0) (0, 0, 0.5)

3.2. Electronic band structure

We show in Fig. 3 the band structures for $BeO_{0.5}S_{0.5}$, $BeO_{0.5}Se_{0.5}$ and $BeO_{0.5}Te_{0.5}$ alloys at the optimized lattice parameters using HSE06 approximation. The bandgap structure prediction displays indirect band gap (R—Γ'*k*-points) semiconductors for $BeO_{0.5}S_{0.5}$ and $BeO_{0.5}Se_{0.5}$ and a metallic demeanor in $BeO_{0.5}Te_{0.5}$. Pristine BeTe binary compound

Table 2
The calculated lattice constant and bulk modulus of $BeO_{1-x}S_x$, $BeO_{1-x}Se_x$ and $BeO_{1-x}Te_x$ alloys along with the available experimental and theoretical data.

	a (Å) Present	a (Å) Exp.	a (Å) Previous	B(GPa) Present	B(GPa) Previous	B' Present	B' Previous
$BeO_{1-x}S_x$							
$x = 0$	3.68	3.79 [41]	3.657 [1], 3.648 [42], 3.651 [43], 3.685 [46]	243.05	231 [42], 244 [1], 232 [43]	4.09	3.64 [1], 3.80 [18]
$x = 0.25$	3.99			183.73		3.7	
$x = 0.5$	4.29			146.33		3.78	
$x = 0.75$	4.44			125.62		3.74	
$x = 1$	4.61		4.64 [44], 4.63 [19], 4.492 [45]	111.27	112 [14], 107 [44], 127.5 [45]	3.73	3.69 [14], 3.4 [44], 3.201 [45]
$BeO_{1-x}Se_x$							
$x = 0.25$	4.09			167.63		3.74	
$x = 0.5$	4.48			130.2		3.84	
$x = 0.75$	4.65			109.83		3.74	
$x = 1$	4.86		4.93 [44], 4.795 [45]	89.33	97 [14], 85 [44], 91.2 [45]	4.43	3.57 [44], 4.032 [45]
$BeO_{1-x}Te_x$							
$x = 0.25$	4.34			137.85		3.53	
$x = 0.5$	4.90			102.46		3.87	
$x = 0.75$	5.09			81.85		4.04	
$x = 1$	5.35		5.37 [44], 5.252 [40]	68.43	71 [14], 65 [44], 79.2 [45]	4.23	3.76 [44], 3.567 [45]

[41] ICSD #26957 and ICDD #01-074-1224.

shows metallic character since the bandgap is closed. Furthermore, the calculated band structures for BeO, BeS, and BeSe binary compounds using HSE06 are given in Fig. S1 (Supporting Information). It can be seen from the binary band structures that the valence band maximum (VBM) and conduction band minimum (CBM) located at the Γ-L'*k*-points for BeO, and at Γ-X' for BeS and BeSe, resulting in indirect bandgap compounds. It is well known that the materials with the indirect band gap are optically inactive due to the phonon contributing to inter band transitions. Thus their applications are limited compared to the direct band gap materials. Interestingly, when chalcogen atoms(S and Se) are substituted the oxygen site in binary BeO at compositions $x = 0.25$, the ternary alloys adopt the direct band gap character with both VBM and CBM are located at the R-R' *k*-points and hence are optically active materials (see-Fig. S2). Therefore, the alloys are expected to be very valuable for the optoelectronic devices working in the UV region. The calculated band gap values using HSE06 and GGA-WC formalisms for all considered concentrations ($0 \leqslant x \leqslant 1$) are summarized in Table 3, along with the previous theoretical [4,43,55,56] results for comparison. It can be seen that the band gap decreases as the x concentration increases. Therefore, these alloys may be of interest for optoelectronics by means of pressure application. Depending on the need and requirement of a specific application, any preferred band gap between 0.32 and 9.21 eV can be attained [57]. According to the data in Table 3, one can observe that the projected values for the band gap utilizing the GGA-WC scheme are underestimated when compared to the calculated ones. It is well identified that in the self-consistent density functional theory, the GGA generally underestimates the energy band gap [58]. This is commonly due to the fact that GGA has simplified formulas that are not satisfactorily flexible to precisely simulate both the exchange–correlation energy and its charge derivative.

The total and partial densities of states (TDOS and PDOS) of these alloys for the GGA-WC case were also considered as depicted in Fig. 4 within the energy interval from (E_F −10 eV) up to (E_F +10 eV). The E_F represents the Fermi level which is set to zero. The upper valence band positioned in the range (−5, −3.9 and −4.6 to E_F) is primarily because of the O-p, Be-p (S-p, Se-p, and Te-p) sites for $BeO_{1-x}S_x$, $BeO_{1-x}Se_x$ and $BeO_{1-x}Te_x$, respectively. The first conduction band positioned in the range from 2.45 to 7.95 eV, 1.7 to 10.8 eV and 0.7 to 0.9 eV is mainly composed of Be and (S, Se, Te) for $BeO_{1-x}S_x$, $BeO_{1-x}Se_x$, and $BeO_{1-x}Te_x$, respectively. The major band gap at equilibrium relates to the electronic transition between (O-p) site to (Be-p) states. There is no intersecting between conduction and valence bands in $BeO_{1-x}S_x$ and $BeO_{1-x}Se_x$, the gap is not weaker and the density of states near the Fermi level has a smaller value. Hence, these show that the reported alloys are semiconductors [56].

3.3. Thermodynamic properties

The thermodynamic results were obtained based on GGA-WC calculations. The phase stability of $BeO_{1-x}A_x$(A = S, Se, Te) solid solutions were resolved using the Gibbs free energy defined according to the following expression [59].

$$\Delta G = \Delta H - T\Delta S \tag{2}$$

where

$$\Delta H = \Omega x(1-x) = E_{Tot}^{BeO1-x(S,Se,Te)_x} - xE_{Tot}^{Be(S,Se,Te)} - (1-x)E_{Tot}^{O(S,Se,Te)} \tag{3}$$

$$\Delta S = -R[x\ln x + (1-x)\ln(1-x)] \tag{4}$$

ΔS and ΔH are mixing entropy and enthalpy of mixing, respectively. Ω is the interaction parameter, $E_{Tot}^{BeO1-x(S,Se,Te)}$, $E_{Tot}^{Be(S,Se,Te)}$ and $E_{Tot}^{O(S,Se,Te)}$ are the total energies of the $BeO_{1-x}A_x$ (A = S, Se, Te) alloys, Be (S, Se, Te), and O (S, Se, Te) binary compounds, while R is the constant of ideal gases and $T$is the absolute temperature.

Using Eq. (3), the achieved interaction parameter Ω values at various concentrations, as depicted in Fig. 5, are well quadratically fitted. Using Eqs. (2)–(4), we projected the x-T phase diagram of the $BeO_{1-x}A_x$ (A = S, Se, Te) alloys. The interaction parameter decreases with increasing x concentration and it increases in the sequences S → Se → Te. The larger enthalpy for $BeO_{1-x}Te_x$ alloy suggests a large value of Ω and therefore, a higher critical temperature [60]. All of the proposed ternary alloys have a positive formation enthalpy, denoting that the studied polymorph is not energetically favorable and cannot be synthesized at normal conditions. This polymorph can be stabilized under extreme conditions of pressure or temperature. This behavior has been confirmed by previous experimental and theoretical investigations [14,16,17]. This conclusion also confirmed in Table 4, as the temperature increase, the free energy F becomes more negative, leading to negative formation enthalpy according to equation (2). Furthermore, Schon [61] found that RS-BeO possesses negative enthalpy at 160 GPa, demonstrating the stability of this polymorph at high pressure.

The binodal curve, which denotes the equilibrium solubility limits versus temperature, can be computed using the common tangent method from the ΔG [62]. As demonstrated in Fig. 6, the critical temperature for particular x concentrations is found to be 145 K, 222 K and 365 K for $BeO_{1-x}S_x$, $BeO_{1-x}Se_x$, and $BeO_{1-x}Te_x$, respectively. These results are similar to the qualitative behavior of other alloys [63–65]. One can perceive that the critical temperatures of the studied alloys are

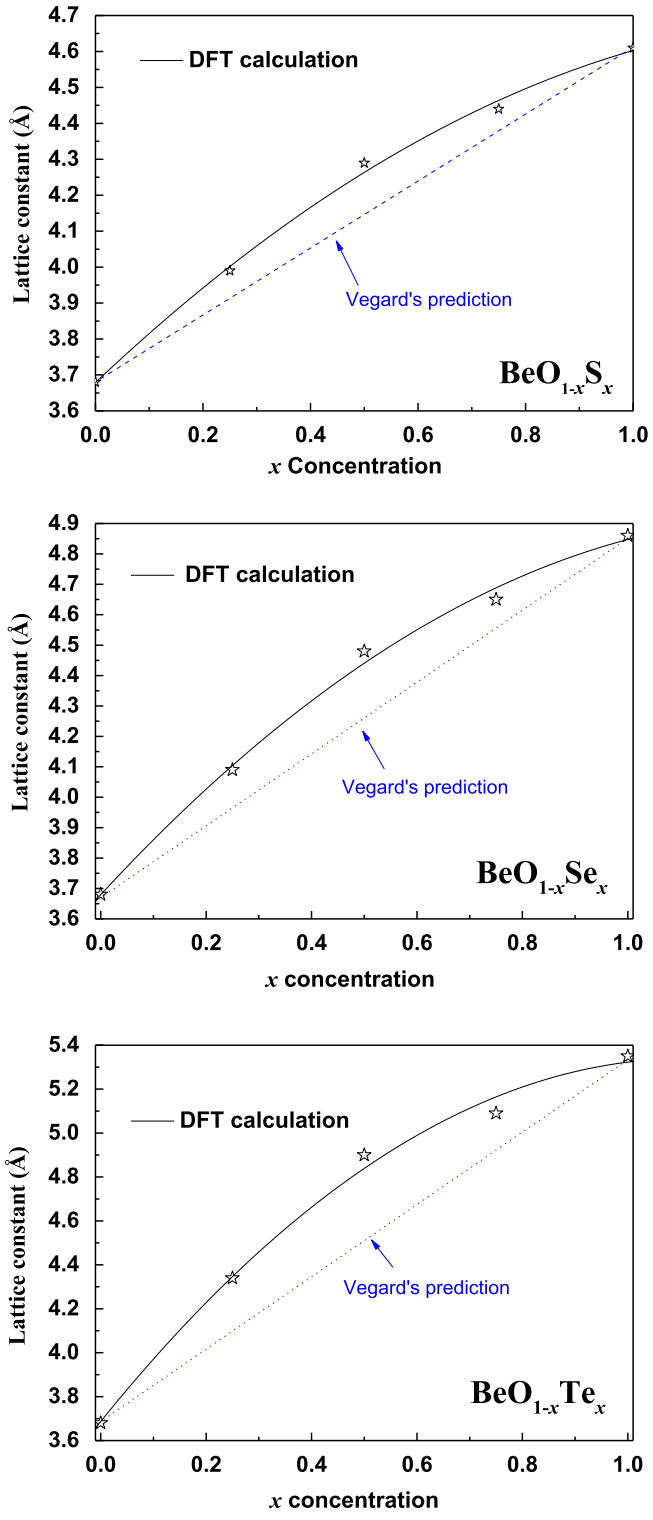

Fig. 1. Lattice constant and its deviation based on Vegard's rule as a function of the *x* fraction in BeO1-xAx (A = S, Se, Te) alloys using GGA-WC.

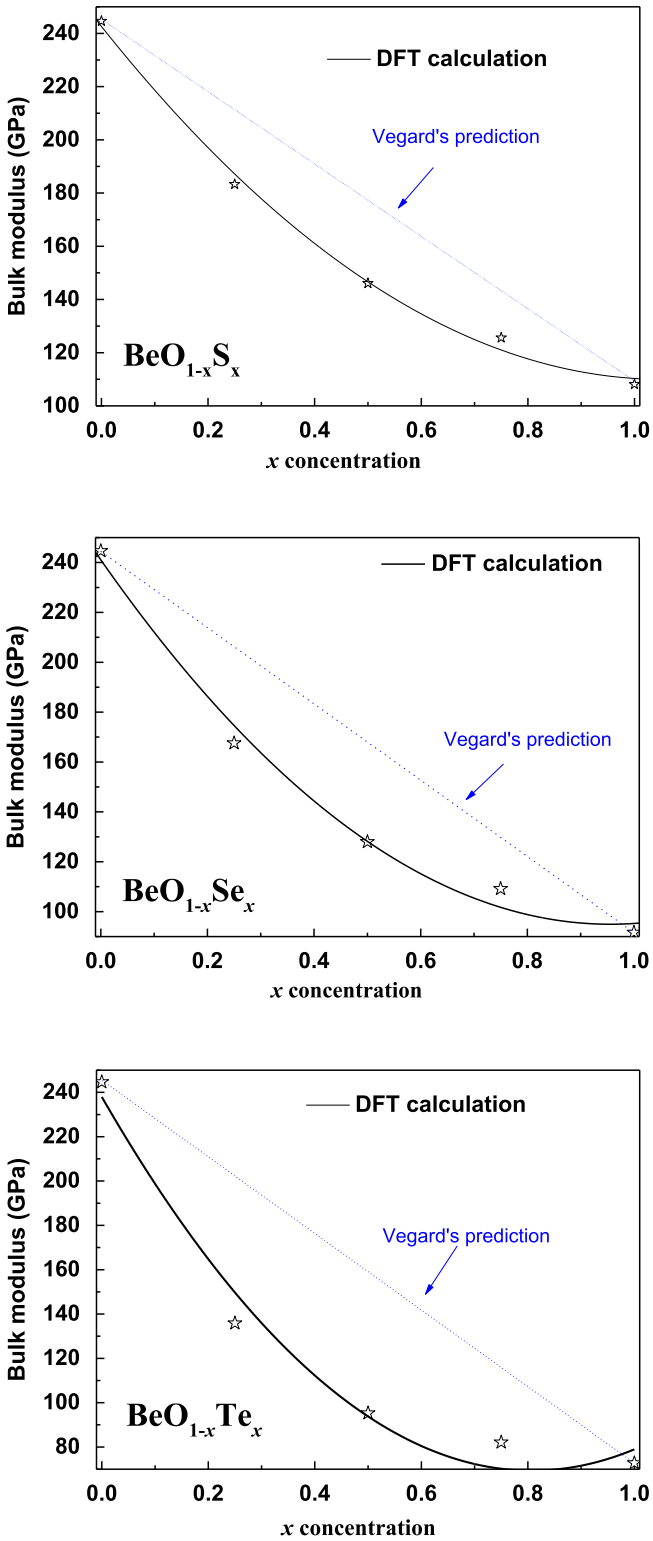

Fig. 2. Bulk modulus and its deviation based on Vegard's rule as a function of the *x* fraction in BeO1-xAx (A = S, Se, Te) alloys using GGA-WC.

low, indicating the easy random mixing of BeO and OA (A = S, Se, and Te). With the spinodal curve, it is possible to draw out the metastability region. The wide range between the bimodal and spinodal curves confirms that the alloys may exist as a metastable phase [63]. These results may suggest that the rocksalt alloys are stable at low temperature. The benefit of metastable alloys within device structures can extend the range of electronic and optical features. The flexibility in materials design accorded by the metastable alloys unfold opportunity for exciting novel device ranges that drives attempts to unravels and promote their production, stabilization, and optimization [66].

To measure the heat capacity of $BeO_{0.5}A_{0.5}$ (A = S, Se, Te) alloys under the effect of high temperature, we have employed the quasi-harmonic Debye model [67]. As a first step, a set of total energy calculation versus primitive cell volume (*E–V*); in the static approximation was performed and fitted with a numerical *EOS*so as to determine its

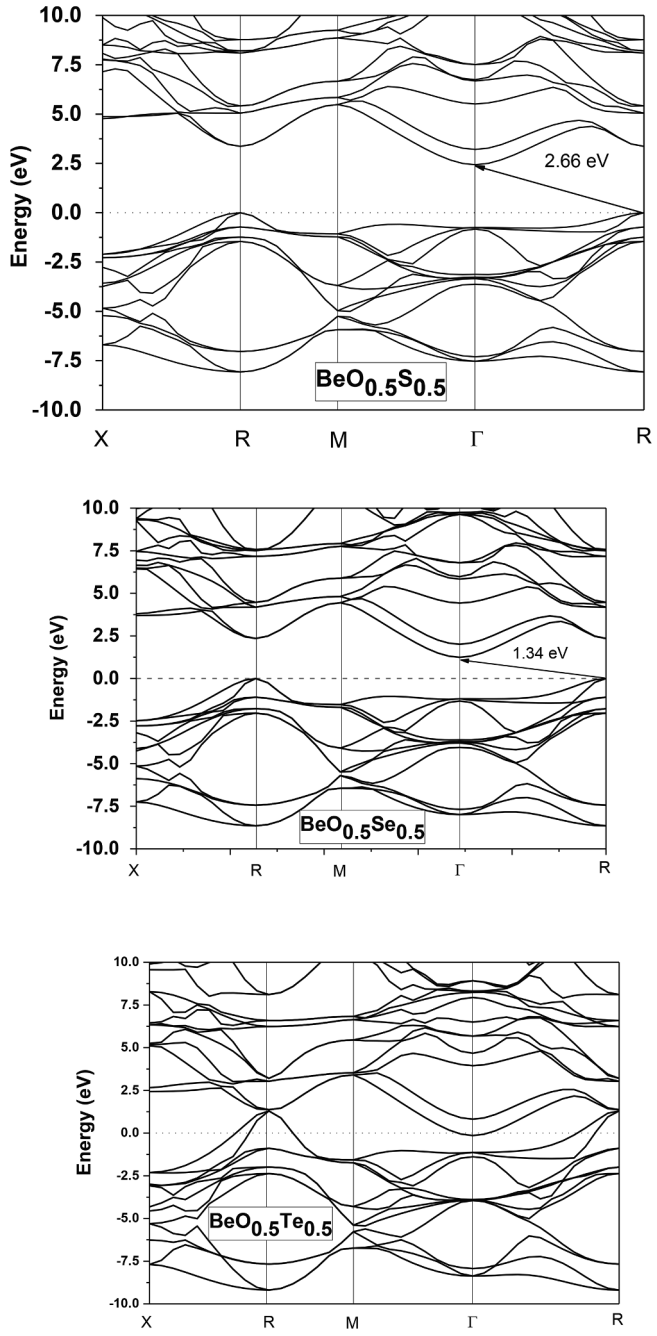

Fig. 3. The band structures of BeO0.5S0.5, BeO0.5Se0.5 and BeO0.5Te0.5 alloys using HSE06 formalism along the high directions X, R, M and Γ points in the first Brillouin zone at the calculated equilibrium lattice constants. The horizontal dotted line designates Fermi level (EF).

structural parameters at P = 0 and T = 0, and then derive the macroscopic features as function of temperature from standard thermodynamic relations. The heat capacity C_V was calculated by the following expression [68]:

$$C_v = 3nk_B\left[4D(\theta_D/T) - \frac{3\theta_D/T}{e^{\theta_D/T} - 1}\right] \quad (5)$$

where n is the number of atoms per formula unit, k_B is the Boltzmann constant and $D(\theta_D/T)$ symbolizes the Debye integral. Fig. 7 exhibits the variation heat capacities C_V as a function of temperature at nil pressure for the binary BeS, BeSe and BeTe compounds and ternary $BeO_{0.5}S_{0.5}$, $BeO_{0.5}Se_{0.5}$ and $BeO_{0.5}Te_{0.5}$ alloys. At higher temperatures, C_V does not have a dependency on temperature and approaches to the Dulong-Petit

Table 3
The calculated band gap of $BeO_{1-x}S_x$, $BeO_{1-x}Se_x$, and $BeO_{1-x}Te_x$ alloys compared with experimental and theoretical data.

	Present (eV) GGA-WC	Present (eV) HSE06	Previous (eV)
$BeO_{1-x}S_x$			
$x = 0$	7.79	9.21	10.96 [4], 9.01 [43], 9.1 [55]
$x = 0.25$	4.06	4.61	
$x = 0.5$	1.65	2.66	
$x = 0.75$	0.58	1.48	
$x = 1$	0.92	2.02	1.15 [55], 0.972 [56]
$BeO_{1-x}Se_x$			
$x = 0.25$	3.48	3.66	
$x = 0.5$	0.83	1.34	
$x = 0.75$	0.00	0.32	
$x = 1$	0.47	0.90	0.4 [55]
$BeO_{1-x}Te_x$			
$x = 0.25$	1.80	2.40	
$x = 0.5$	0.00	0.00	
$x = 0.75$	0.00	0.00	
$x = 1$	0.00	0.00	−0.8 [55]

[69] limit and is equivalent to ~50 J.mol^{-1}.K^1 for parent oxides and ~49.5 J.mol^{-1}.K^{-1}for ternary alloys. There is no available experimental or theoretical data for comparison, then our results are predictions. Furthermore, these results agree well with the heat capacity values of WZ-BeO and ZB-BeX (X = S, Se, Te) [14,70,71]. We reported in Table 4 the computed heat capacities C_V (Jmol^{-1}.K^{-1}), entropy S (J mol^{-1}.K^{-1})and free energy F (J mol^{-1}) for BeO, $BeO_{0.5}S_{0.5}$,$BeO_{0.5}Se_{0.5}$ and $BeO_{0.5}Te_{0.5}$ at various temperatures.

3.4. Optical properties

It is important to study the optical functions since they deliver meaningful evidence about the electronic structure of solids [72]. The optical features of solids are typically recognized using the complex dielectric function $\varepsilon(\omega) = \varepsilon_1(\omega) + i\varepsilon_2(\omega)$, which signifies the electronic band structure [73]. The Kramers-Kronig relation was used to calculate the real part $\varepsilon_1(\omega)$ from the imaginary part [74]. The momentum matrix elements between the unoccupied and occupied electronic states can be employed to evaluate the imaginary part $\varepsilon_2(\omega)$ [75]. Detail descriptions of the schemes utilized to estimate the optical features can be found in Ref. [48] and references therein. The refractive index $n(\omega)$ of the semiconducting solids is an essential parameter in defining the optical and electric characteristics of the crystal [76]. Furthermore, understanding of the refractive index is necessary for devices like waveguides, detectors, solar cells and photonic crystals [77]. The value of $n(\omega)$ can be calculated from the dielectric function by means of the given expression [78].

$$n(\omega) = \left[\frac{\varepsilon_1(\omega)}{2} + \frac{\sqrt{\varepsilon_1^2(\omega) + \varepsilon_2^2(\omega)}}{2}\right]^{1/2} \quad (6)$$

The refractive index satisfies the relation $n(0) = \varepsilon^{1/2}(0)$ [79] at low frequency. We listed in Table 5 the band gap, real part of the dielectric function, reflectivity, refractive index, critical value of the absorption coefficient and conductivity at zero frequency for $BeO_{1-x}S_x$, $BeO_{1-x}Se_x$ and $BeO_{1-x}Te_x$. Zero frequency limit $\varepsilon_1(0)$ is the most significant quantity for the real part $\varepsilon_1(\omega)$ of the dielectric function $\varepsilon(\omega)$, which is the electronic part of the static dielectric constant and depends strongly on the bandgap [74]. We remark that the alloys with small band gap yield a larger static dielectric constants $\varepsilon_1(0)$. This can be described on the basis of the Penn model $\varepsilon_1(0) = 1 + (\hbar\omega_p/E_g)^2$ [80]. The obtained values are consistent with previous theoretical reports [4].

The absorption spectra for parent oxides and ternary alloys are depicted in Fig. 8. It can be seen that all ternary alloys have two bands

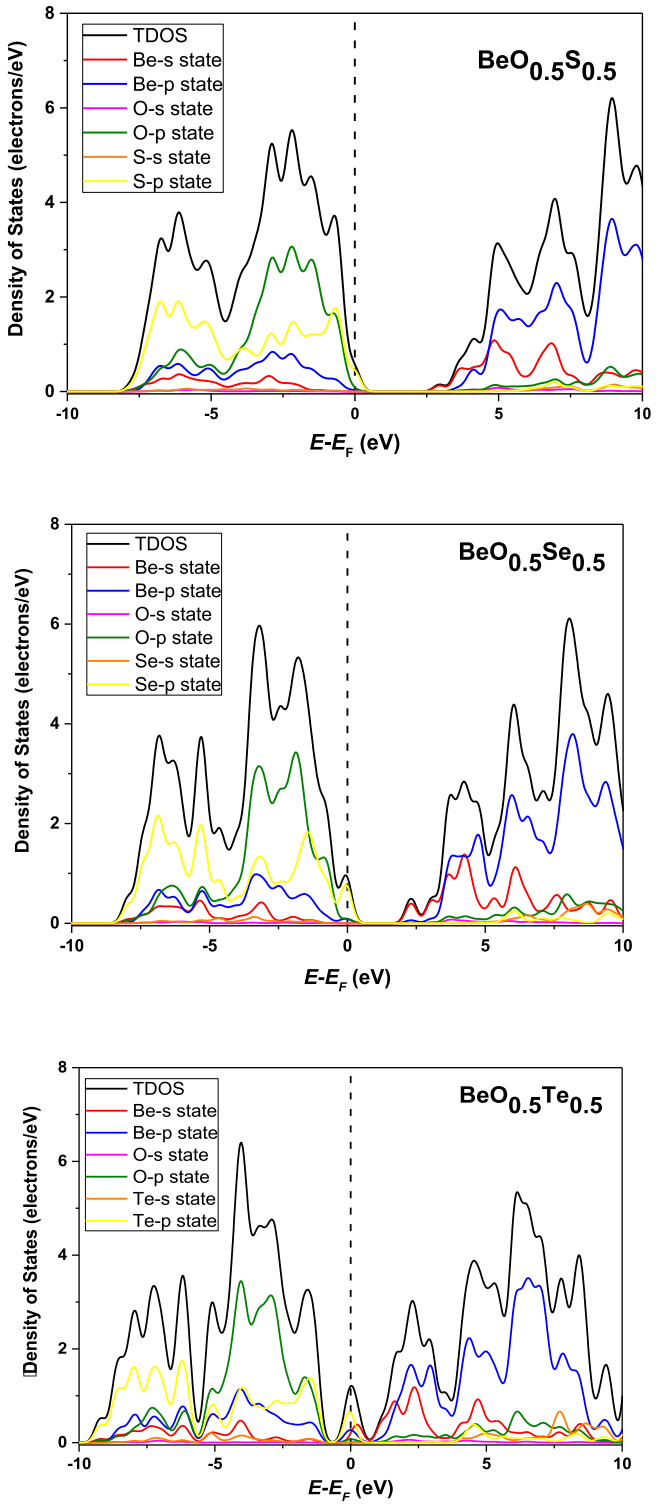

Fig. 4. The total and atomic site projected densities of states (TDOS and PDOS) of BeO0.5S0.5, BeO0.5Se0.5 and BeO0.5Te0.5 alloys using GGA-WC formalism. The vertical dashed line designates Fermi level (EF).

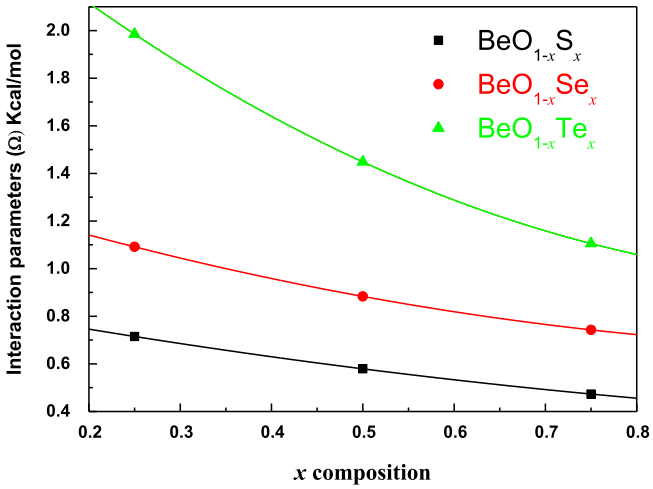

Fig. 5. The interaction parameter calculated using the GGA-WC scheme as a function of composition.

Table 4
Calculated heat capacities C_V (Jmol^{-1}.K^{-1}), entropy S (Jmol^{-1}.K^{-1}) and free energy F (Jmol^{-1}) for BeO, $BeO_{0.5}S_{0.5}$,$BeO_{0.5}Se_{0.5}$ and $BeO_{0.5}Te_{0.5}$ binary and ternary alloys at various temperatures.

	C_V (Jmol^{-1}.K^{-1})	S(Jmol^{-1}.K^{-1})	F(Jmol^{-1})
T = 100 K			
BeO	12.40	17.69	12991.1
$BeO_{0.5}S_{0.5}$	30.67	48.43	3185.35
$BeO_{0.5}Se_{0.5}$	20.25	136.28	8208.4
$BeO_{0.5}Te_{0.5}$	30.67	48.43	3185.35
T = 300 K			
BeO	36.42	45.24	6615.75
$BeO_{0.5}S_{0.5}$	46.00	91.93	−11359.50
$BeO_{0.5}Se_{0.5}$	43.93	50.57	1324.97
$BeO_{0.5}Te_{0.5}$	46.00	91.93	−11359.5
T = 500			
BeO	43.78	65.90	−4611.84
$BeO_{0.5}S_{0.5}$	48.83	116.13	−32351.66
$BeO_{0.5}Se_{0.5}$	47.53	75.54	−11604.1
$BeO_{0.5}Te_{0.5}$	48.38	116.13	−32351.6
T = 700			
BeO	46.52	81.13	−19385.7
$BeO_{0.5}S_{0.5}$	49.10	131.84	−55985.6
$BeO_{0.5}Se_{0.5}$	48.65	91.04	−28417.6
$BeO_{0.5}Te_{0.5}$	49.10	132.54	−57307.5
T = 900			
BeO	47.78	92.99	−36843.5
$BeO_{0.5}S_{0.5}$	49.41	144.92	−85105.8
$BeO_{0.5}Se_{0.5}$	49.13	104.03	−48045.2
$BeO_{0.5}Te_{0.5}$	49.41	144.92	−85105.8

which correspond mainly to the transition from O-2p (VB) to the unoccupied Be-p (CB) states. It is also seen in Fig. 8 that the peaks of the absorption (imaginary part) of the BeO, BeS, BeSe, BeTe, $Be_{0.5}O_{0.5}Te_{0.5}$, $Be_{0.5}O_{0.5}Se_{0.5}$, $Be_{0.5}O_{0.5}S_{0.5}$ compounds shifted toward lower energies (red-shift) by augmenting the x concentration. This trend is similar to the decreasing of the band gap with increasing x amount. In Table 5, one can perceive that the refractive index and reflectivity at zero frequency follow the same trend of the static dielectric constant $\varepsilon_1(0)$ with increasing x values. Furthermore, the critical values of the absorption coefficient and conductivity decrease as the x concentration increased which are of consistent with the vary of the band gap values listed in Table 3.

In Fig. 9, we show the loss function of BeO, BeS, BeSe, BeTe, $Be_{0.5}O_{0.5}S_{0.5}$, $Be_{0.5}O_{0.5}Se_{0.5}$ and $Be_{0.5}O_{0.5}Te_{0.5}$ as a function of energy. The energy loss function is a vital factor describing the energy loss of a fast electron traversing of the material [81]. The peak in energy loss

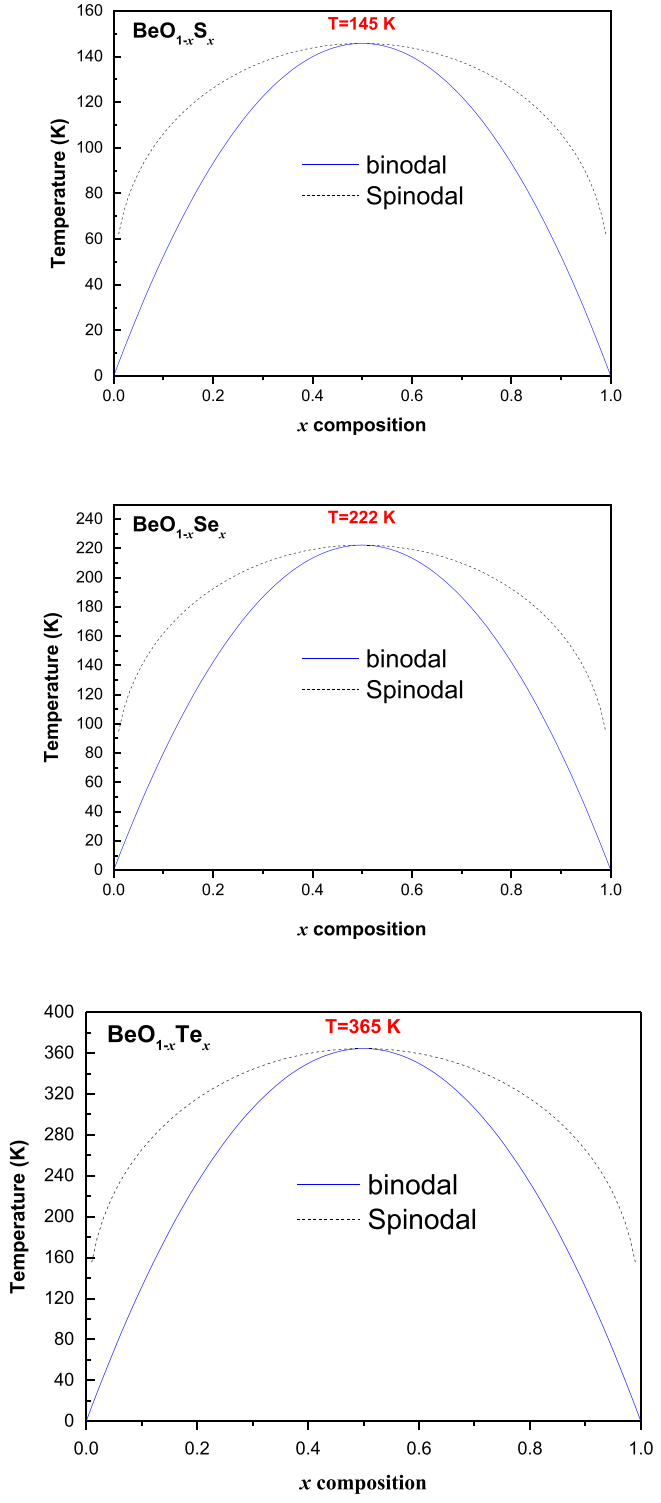

Fig. 6. The predicted x-T phase diagram of the BeO1-xAx (A = S, Se, Te) alloys based on GGA-WC.

function occurs at about 32.7 eV, 19.8 eV, 20.8 eV and 18.9 eV for BeO, BeS, BeSe and BeTe, respectively, while at about 21.4 eV, 23.6 eV and 22.04 eV for $Be_{0.5}O_{0.5}S_{0.5}$, $Be_{0.5}O_{0.5}Se_{0.5}$ and $Be_{0.5}O_{0.5}Te_{0.5}$, respectively. This indicates that the S, Se, and Te alloying BeO makes the main peaks to shift toward lower energy values, and the intensity decreases

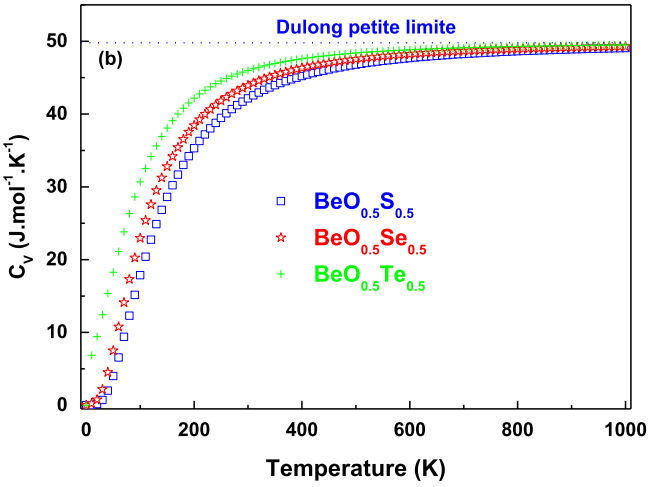

Fig. 7. Displays the heat capacities CV versus temperature up to T = 1000 K at zero pressure for (a) the binary BeS, BeSe and BeTe compounds and (b) for ternary BeO0.5A0.5 (A = S, Se, Te) alloys based on GGA-WC calculations.

Table 5
The calculated energy gap Eg, static dielectric constant ε1(0), reflectivity R (0), refractive index n(0), the critical values of the absorption coefficient (A) and conductivity for BeO1-xSx, BeO1-xSex and BeO1-xTex alloys using GGA-WC formalism.

	E_g (eV)	$\varepsilon_1(0)$	R (0) (%)	n(0)	A (critical value)	Conductivity (critical value)
$BeO_{1-x}S_x$						
$x = 0$	7.79	3.82	10.43	1.95	7.01	6.91
$x = 0.25$	4.06	5.24	15.36	2.28	3.55	3.51
$x = 0.5$	1.65	7.12	20.66	2.66	2.53	2.44
$x = 0.75$	0.58	8.85	24.68	2.97	1.97	1.78
$x = 1$	0.92	9.92	26.84	3.15	2.91	2.85
$BeO_{1-x}Se_x$						
$x = 0.25$	3.48	5.48	16.13	2.34	3.05	2.89
$x = 0.5$	0.83	8.19	23.24	2.86	2.08	1.87
$x = 0.75$	0.00	10.54	27.99	3.24	1.64	1.27
$x = 1$	0.47	12.01	30.49	3.46	2.25	2.19
$BeO_{1-x}Te_x$						
$x = 0.25$	1.80	6.77	19.79	2.60	1.78	1.62
$x = 0.5$	0.00	11.45	29.57	3.38	0.61	0.49
$x = 0.75$	0.00	26.65	45.78	5.16	0.01	0.01
$x = 1$	1.32	18.29	38.57	4.27	1.05	0.96

with increasing the x concentrations. Furthermore, the obtained optical data of the studied compounds are in reasonable agreement with previous theoretical reports [4,43,55,82].

4. Conclusions

We applied ab initio analysis using GGA-WC and HSE06 approximations in details for the structural, electronic, and optical properties of binary and ternary chalcogenide alloys $BeO_{1-x}S_x$, $BeO_{1-x}Se_x$, and $BeO_{1-x}Te_x$. The structural parameters are in acceptable agreement with the current theoretical and experimental records using GGA-WC. The lattice constant and bulk modulus values vary non-linearly as the x concentration increased. It is evidence that the binary compounds BeO, BeS and BeSe exhibit an indirect band gap while the ternary alloys BeOA (A = S and Se) at $x = 0.25$ exhibit a direct band gap. Furthermore, the BeOTe alloys exhibit metallic behavior, except at $x = 0.25$, where an indirect band gap has occurred. It can be

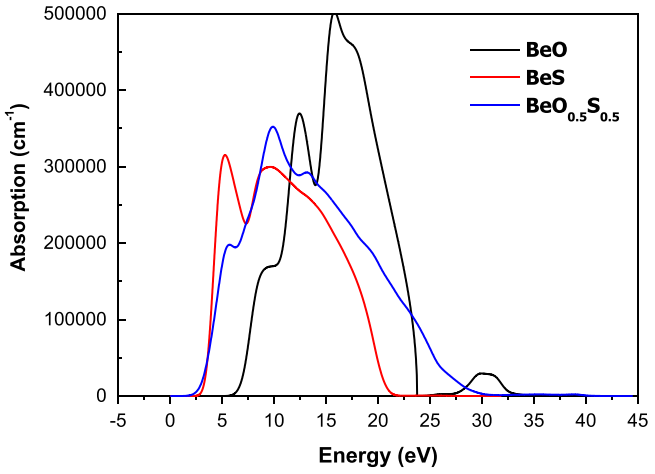

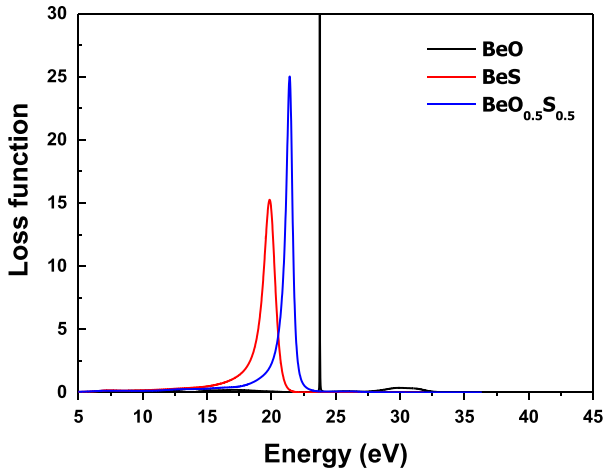

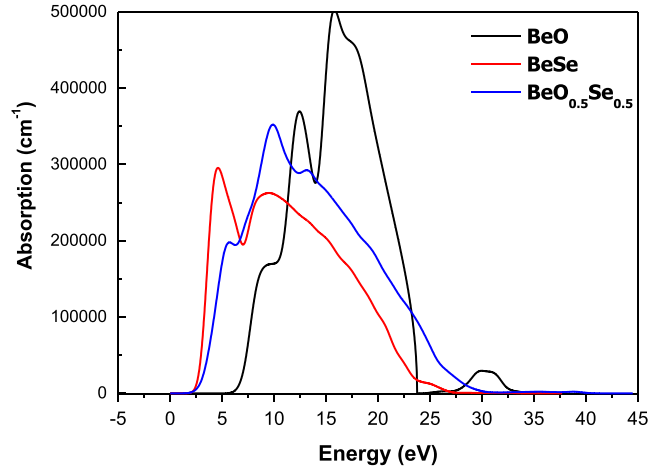

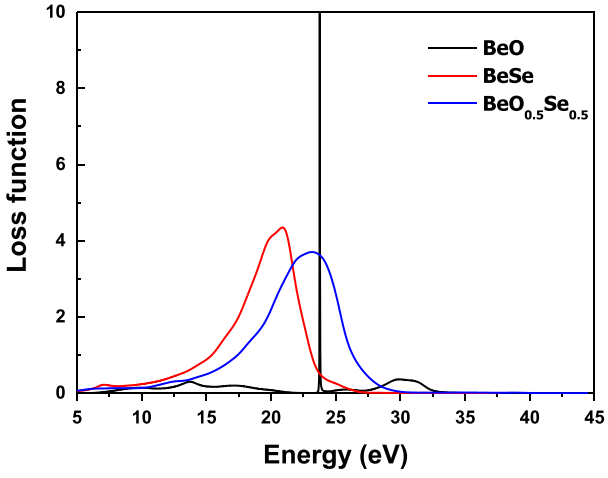

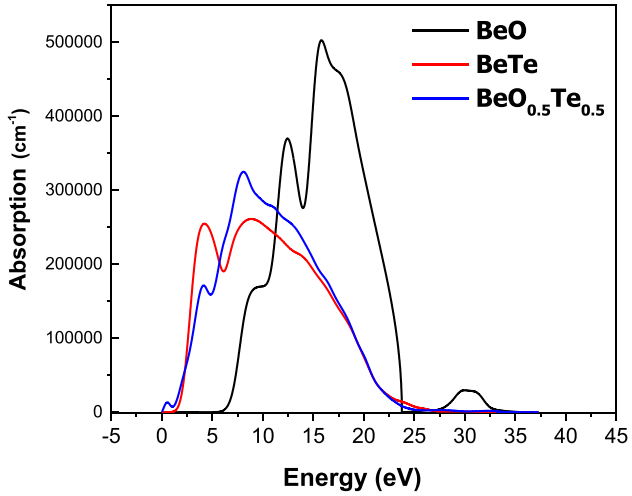

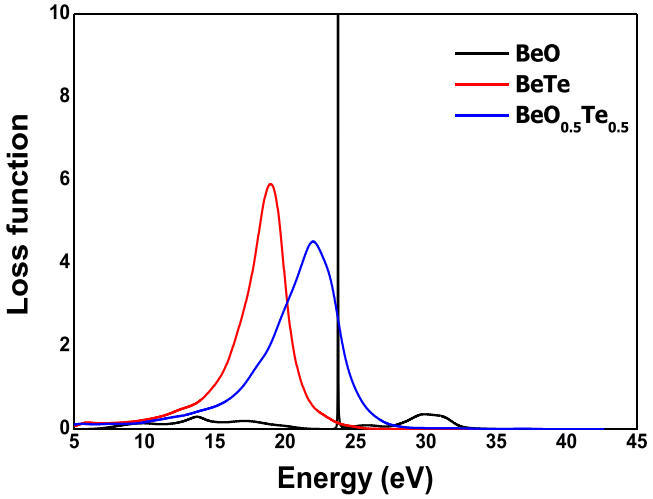

Fig. 8. The absorption versus energy for the binary BeO, BeS, BeSe and BeTe compounds and ternary BeO0.5S0.5, BeO0.5Se0.5 and BeO0.5Te0.5 alloys based on GGA-WC calculations.

Fig. 9. The loss function versus energy for the binary BeO, BeS, BeSe and BeTe compounds and ternary BeO0.5S0.5, BeO0.5Se0.5 and BeO0.5Te0.5 alloys based on GGA-WC calculations.

determined that the ternary alloys can be utilized in optoelectronics working in the UV, visible, and IR regions. The dielectric constant, refractive index and reflectivity at zero frequency using GGA-WC increase with increasing of x concentration. Furthermore, the negative value of the real part shifts toward lower energies with increasing x concentration for all ternary alloys. The same trend can also be seen for the imaginary part. Furthermore, the critical value of the absorption coefficient and conductivity decrease as the x concentration increased.

Finally, the considered phase diagrams specify that the ternary alloys are stable at a relatively low temperature.

Appendix A. Supplementary data

Supplementary data to this article can be found online at https://doi.org/10.1016/j.chemphys.2019.110414.

References

[1] B.-R. Yu, J.-W. Yang, H.-Z. Guo, G.-F. Ji, X.-R. Chen, Phys. B 404 (2009) 1940.
[2] S. Lakel, F. Elhamra, K. Almi, Phys. Status Solidi (b) 255 (2018) 1700524.
[3] H. Xiao, G. Duan, X. Zu, W.J. Weber, J. Mater. Sci. 46 (2011) 6408.
[4] D. Groh, R. Pandey, M.B. Sahariah, E. Amzallag, I. Baraille, M. Rerat, J. Phys. Chem. Solids 70 (2009) 789.
[5] I. Zhezherun, I. Sadikov, V. Taraban'ko, A. Chernyshov, Soviet Atom. Energy 13 (1963) 860.
[6] D. Koh, J.-H. Yum, S.K. Banerjee, T.W. Hudnall, C. Bielawski, W.A. Lanford, B.L. French, M. French, P. Henry, H. Li, J. Vac. Sci. Technol. B Nanotechnol. Microelectron.: Mater., Process., Measure., Phenom. 32 (2014) 03D117.
[7] T. Peltier, R. Takahashi, M. Lippmaa, Appl. Phys. Lett. 104 (2014) 231608.
[8] D. Li, P. Zhang, J. Yan, Sci. Rep. 4 (2014).
[9] U.K. Sakalle, A. Singh, E. Sharma, Bull. Mater. Sci. 37 (2014) 1339.
[10] I. Al-Qasir, N. Jisrawi, V. Gillette, A. Qteish, Ann. Nucl. Energy 87 (2016) 242.
[11] F.E.H. Hassan, H. Akbarzadeh, Comput. Mater. Sci. 35 (2006) 423.
[12] L. Guo, G. Hu, S. Zhang, W. Feng, Z. Zhang, J. Alloys Compd. 561 (2013) 16.
[13] G. Srivastava, H. Tütüncü, N. Günhan, Phys. Rev. B 70 (2004) 085206.
[14] S. Dabhi, V. Mankad, P.K. Jha, J. Alloys Compd. 617 (2014) 905.
[15] D. Rached, M. Rabah, N. Benkhettou, R. Khenata, B. Soudini, Y. Al-Douri, H. Baltache, Comput. Mater. Sci. 37 (2006) 292.
[16] M.B. Sahariah, S. Ghosh, J. Appl. Phys. 107 (2010) 083520.
[17] Y. Mori, T. Ikai, K. Takarabe, A.L. Ruoff, Photon Factory Activity Report, (2003).
[18] P. Van Camp, V. Van Doren, J. Phys.: Condens. Matter 8 (1996) 3385.
[19] K.-L. Wang, S.-P. Gao, J. Phys. Chem. Solids 118 (2018) 242.
[20] Y. Wang, J. Wang, W. Wang, Z. Mei, S. Shang, L. Chen, Z. Liu, J. Phys.: Condens. Matter 22 (2010) 202201.
[21] Z.-C. Guo, F. Luo, G.-F. Ji, L.-C. Cai, Y. Cheng, Phys. B 438 (2014) 60.
[22] E. Wrasse, R. Baierle, Phys. Procedia 28 (2012) 79.
[23] R. Thapa, M. Ghimire, Indian J. Phys. 85 (2011) 727.
[24] M.M. Obeid, S.J. Edrees, M.M. Shukur, Superlattices Microstruct. 122 (2018) 124.
[25] M.M. Obeid, Y. Mogulkoc, S.J. Edrees, Y. Ciftci, M.M. Shukur, M.H. Al-Marzooqee, Mater. Res. Bull. 108 (2018) 255.
[26] K. Mun Wong, S. Alay-e-Abbas, Y. Fang, A. Shaukat, Y. Lei, J. Appl. Phys. 114 (2013) 034901.
[27] K.M. Wong, W. Khan, M. Shoaib, U. Shah, S.H. Khan, G. Murtaza, J. Electron. Mater. 47 (2018) 566.
[28] M.M. Obeid, H.R. Jappor, S.J. Edrees, M.M. Shukur, R. Khenata, Y. Mogulkoc, J. Mol. Graph. Model. 89 (2019) 22.
[29] D. Hoat, T.V. Vu, M.M. Obeid, H.R. Jappor, Superlattices Microstruct. (2019).
[30] H.R. Jappor, M.M. Obeid, T.V. Vu, D. Hoat, H.D. Bui, N.N. Hieu, S.J. Edrees, Y. Mogulkoc, R. Khenata, Superlattices Microstruct. (2019).
[31] S.J. Clark, M.D. Segall, C.J. Pickard, P.J. Hasnip, M.I. Probert, K. Refson, M.C. Payne, Z. Kristallogr. –Crystall. Mater. 220 (2005) 567.
[32] Z. Wu, R.E. Cohen, Phys. Rev. B 73 (2006) 235116.
[33] H.J. Monkhorst, J.D. Pack, Phys. Rev. B 13 (1976) 5188.
[34] T.H. Fischer, J. Almlof, J. Phys. Chem. 96 (1992) 9768.
[35] J. Heyd, G.E. Scuseria, M. Ernzerhof, J. Chem. Phys. 118 (2003) 8207.
[36] J. Heyd, G.E. Scuseria, M. Ernzerhof, J. Chem. Phys. 124 (2006) 219906.
[37] A. Zunger, S.-H. Wei, L. Ferreira, J.E. Bernard, Phys. Rev. Lett. 65 (1990) 353.
[38] C. Jiang, Acta Mater. 57 (2009) 4716.
[39] G. Murtaza, R. Khenata, A. Safeer, Z. Alahmed, S.B. Omran, Comput. Mater. Sci. 91 (2014) 43.
[40] M. Rashid, N. Noor, B. Sabir, S. Ali, M. Sajjad, F. Hussain, N. Khan, B. Amin, R. Khenata, Comput. Mater. Sci. 91 (2014) 285.
[41] W. Gerlach, Z. Phys. 9 (1922) 184.
[42] C.-J. Park, S.-G. Lee, Y.-J. Ko, K. Chang, Phys. Rev. B 59 (1999) 13501.
[43] B. Amrani, F.E.H. Hassan, H. Akbarzadeh, J. Phys.: Condens. Matter 19 (2007) 436216.
[44] A. Berghout, A. Zaoui, J. Hugel, J. Phys.: Condens. Matter 18 (2006) 10365.
[45] A. Munoz, P. Rodriguez-Hernandez, A. Mujica, Phys. Rev. B 54 (1996) 11861.
[46] Y. Cai, S. Wu, R. Xu, J. Yu, Phys. Rev. B 73 (2006) 184104.
[47] L. Vegard, Z. Phys. 5 (1921) 17.
[48] B. Khalfallah, F.D. Khodja, B. Doumi, M. Berber, A. Mokaddem, A. Bentayeb, J. Comput. Electron. (2018) 1.
[49] M. Labidi, S. Labidi, S. Ghemid, H. Meradji, F.E.H. Hassan, Phys. Scr. 82 (2010) 045605.
[50] S. Drablia, N. Boukhris, R. Boulechfar, H. Meradji, S. Ghemid, R. Ahmed, S.B. Omran, F.E.H. Hassan, R. Khenata, Phys. Scr. 92 (2017) 105701.
[51] J. Dismukes, L. Ekstrom, R. Paff, J. Phys. Chem. 68 (1964) 3021.
[52] B. Jobst, D. Hommel, U. Lunz, T. Gerhard, G. Landwehr, Appl. Phys. Lett. 69 (1996) 97.
[53] F. Birch, Phys. Rev. 71 (1947) 809.
[54] S. Labidi, M. Labidi, H. Meradji, S. Ghemid, F.E.H. Hassan, Comput. Mater. Sci. 50 (2011) 1077.
[55] R. Ali, S. Mohammad, H. Ullah, S. Khan, H. Uddin, M. Khan, N. Khan, Phys. B 410 (2013) 93.
[56] F. Wang, C. Hu, J. Wu, P. Zhou, Z. Zheng, C. Hu, Euro. Phys. J. Appl. Phys. 62 (2013) 20103.
[57] I. Khan, I. Ahmad, B. Amin, G. Murtaza, Z. Ali, Phys. B 406 (2011) 2509.
[58] V. Fiorentini, A. Baldereschi, Phys. Rev. B 51 (1995) 17196.
[59] L. Ferreira, S.-H. Wei, A. Zunger, Phys. Rev. B 40 (1989) 3197.
[60] F.E.H. Hassan, B. Amrani, J. Phys.: Condens. Matter 19 (2007) 386234.
[61] J. Schön, Z. Anorg. Allg. Chem. 630 (2004) 2354.
[62] K. Hacini, Z. Chouahda, A. Djedid, H. Meradji, S. Ghemid, F.E.H. Hassan, R. Khenata, Mater. Sci. Semicond. Process. 26 (2014) 642.
[63] N. Boukhris, H. Meradji, S. Ghemid, S. Drablia, F.E.H. Hassan, Phys. Scr. 83 (2011) 065701.
[64] M. Labidi, H. Meradji, S. Ghemid, S. Labidi, F. El Haj Hassan, Mod. Phys. Lett. B 25 (2011) 473.
[65] S. Labidi, H. Meradji, S. Ghemid, M. Labidi, F.E.H. Hassan, J. Phys.: Condens. Matter 20 (2008) 445213.
[66] T.F. Kuech, S.E. Babcock, L. Mawst, Appl. Phys. Rev. 3 (2016) 040801.
[67] M. Blanco, A.M. Pendás, E. Francisco, J. Recio, R. Franco, J. Mol. Struct. (Thoechem) 368 (1996) 245.
[68] X. Wang, H. Khachai, R. Khenata, H. Yuan, L. Wang, W. Wang, A. Bouhemadou, L. Hao, X. Dai, R. Guo, Sci. Rep. 7 (2017) 16183.
[69] A. Petit, P. Dulong, Ann. Chim. Phys. 10 (1819) 395.
[70] Y.N. Makurin, I. Shein, M. Gorbunova, V. Kiiko, A. Ivanovskii, Refract. Ind. Ceram 47 (2006) 310.
[71] C. Jing, C. Xiang-Rong, Z. Wei, Z. Jun, Chin. Phys. B 17 (2008) 1377.
[72] M.A. Rahman, M.Z. Rahaman, M.A.R. Sarker, Comput. Condens. Matter 9 (2016) 19.
[73] L. Qi-Jun, Z. Ning-Chao, L. Fu-Sheng, L. Zheng-Tang, Chin. Phys. B 23 (2014) 047101.
[74] N. Singh, P.K. Singh, A. Shukla, S. Singh, P. Tandon, J. Inorg. Organomet. Polym Mater. 26 (2016) 1413.
[75] Y.-M. Shi, S.-L. Ye, J. Central South Univ. Technol. 18 (2011) 998.
[76] X. Li, H. Cui, R. Zhang, Sci. Rep. 6 (2016).
[77] N. Ravindra, P. Ganapathy, J. Choi, Infrared Phys. Technol. 50 (2007) 21.
[78] S. Saha, T. Sinha, A. Mookerjee, Phys. Rev. B 62 (2000) 8828.
[79] S.J. Edrees, M.M. Shukur, M.M. Obeid, Comput. Condens. Matter 14 (2018) 20.
[80] D.R. Penn, Phys. Rev. 128 (1962) 2093.
[81] A. Bouhemadou, R. Khenata, Comput. Mater. Sci. 39 (2007) 803.
[82] C. Okoye, Euro. Phys. J. B-Condens. Matter Complex Syst. 39 (2004) 5.